DETECTION OF MODULATED SIGNALS USING CYCLOSTATIONARY PROPERTY

A Project Report

submitted by

KIRANKUMAR ALLUVADA

in partial fulfilment of the requirements
for the award of the degree of

MASTER OF TECHNOLOGY

DEPARTMENT OF ELECTRICAL ENGINEERING
INDIAN INSTITUTE OF TECHNOLOGY MADRAS.

May 2013

THESIS CERTIFICATE

This is to certify that the thesis titled **DETECTION OF MODULATED SIGNALS USING CYCLOSTATIONARY PROPERTY**, submitted by **KIRANKUMAR ALLUVADA**, to the Indian Institute of Technology, Madras, for the award of the degree of **Master of Technology**, is a bonafide record of the research work done by him under our supervision. The contents of this thesis, in full or in parts, have not been submitted to any other Institute or University for the award of any degree or diploma.

Prof. Devendra Jalihal
Project Guide
Professor
Dept. of Electrical Engineering
IIT-Madras, 600 036

Place: Chennai

Date: May 2013

ACKNOWLEDGEMENTS

First and foremost I am deeply indebted to my guide Prof. Devendra Jalihal for his guidance and continuous support throughout this project. I feel honoured and encouraged to have worked under his guidance.

I would also like to take this opportunity to thank my professors at IIT Madras, Prof. David Koilpillai, Prof. R. Aravind, Prof. A.N. Rajagopalan, Prof. K. Giridhar, Dr. Srikrishna Bhashyam, Dr. Arun Pachai Kannu and all other Communications faculty who have imparted knowledge and have motivated me to learn the intricacies of the subjects.

I would like to thank my friends and labmates for their support and encouragement, especially Jagdeesh who helped me many times with Wireless communications. My stay at IITM would remain as most memorable part of my life.

Any amount of thanks to my family, for their love, support and encouragement will never be sufficient to express my gratitude. I would like to dedicate my work to them.

ABSTRACT

KEYWORDS: Cyclostationary ; Cognitive Radio; Spectrum sensing

Spectrum sensing is one of the challenging problems in Cognitive Radio design. The detection and classification of low SNR signals have the most importance in spectrm sensing. The cyclostationarity property of modulated signals is discussed through the simulations. A cyclostationary detector has been implemented to exploit the hidden periodicity of modulated signals and to detect them even under low signal-to-noise ratio (SNR). The detector performance is simulated for OFDM signals in single-tap and multi-tap channels and a few improvements are shown to increase the detector performance.

TABLE OF CONTENTS

LIST OF FIGURES

ABBREVIATIONS

3GPP	3rd Generation Partnership Project
CAF	Cyclic Autocorrelation Function
CF	Cyclic frequency
CP	Cyclic Prefix
DL	Downlink
FAM	FFT Accumulation method
FDD	Frequency Division Duplex
LTE	Long term Evolution
MBSFN	Multicast Broadcast Single Frequency Network
OFDMA	Orthogonal Frequency Division Multiple Access
RS	Reference Signals
SCD	Spectral Correlation denisity
SC-FDMA	Single Carrier- Frequency Division Multiple Access
TDD	Time Division Duplex
UE	User Equipment
UL	Uplink

NOTATIONS

$R_x^\alpha(\tau)$	Cyclic autocorrelation funtion
$S_x^\alpha(f)$	Spectral correlation function
α	Cyclic frequency
$\Delta\alpha$	Cyclic frequency resolution
Δf	Spatial frequency resolution
f_{UL}	Uplink frequency
f_{DL}	Downlink frequency
N_{symb}^{DL}	No. of OFDM symbols per slot in Downlink
N_{RB}^{DL}	No. of physical resource blocks in Downlink
N_{RB}^{sc}	No. of subcarriers per resource block

CHAPTER 1

Introduction

The available Radio spectrum is limited. As there is an increase in number of wireless devices, it is important to utilize the available spectrum efficiently. In the present scenario it has been found that these allocated Radio spectrums are underutilized and are free 15% to 85% most of the time. This issue in wireless communications can be solved in a better way using Cognitive Radio.

The most challenging problem in Cognitive radio is the detection of unused frequency bands. The detector must be able to efficiently intercept the primary user signals even under the low SNR conditions and in the fading environments. A simple detector is Energy detector as it doesn't require any prior knowledge about primary user, but it fails under low SNR conditions. The Cyclostationary detector is proved to be perform better than the Energy detector under low SNR regions. It detects the signals by exploiting the Cyclostationary property which may be caused by modulation or coding, or it may be also intentionally produced.

1.1 Organization of thesis

The Cyclostationary property of signals is explained in Chapter 2. The Cyclic Autocorrelation function, which is used in the detection of modulated signals is defined.

In Chapter 3, FAM algorithm has been implemented which is used to plot the Spectral Correlation Denisity of signals. SCD of some modulated signals are plotted using FAM algorithm, and the cyclostationary property is observed.

In Chapter 4, LTE OFDM signal model is presented, and the frame and slot structures of LTE signals are discussed.

In Chapter 5, Detection of LTE signal is carried out using Cyclic Autocorrelation function.

In Chapter 6, OFDM signal detection is performed using CAF, for different decimation ratios and different sensing times. Blind detection of FFT length of OFDM signals is also presented. The detection performance in multi-path channels is verified.

In Chapter 7, the conclusion of this thesis and future scope is presented.

CHAPTER 2

Cyclostationary property of signals

2.1 What is Cyclostationarity?

A signal is cyclostationary of order n (in the wide sense) if and only if we can find some nth-order non linear transformation of the signal that will generate finite-strength additive sine-wave components, which results in spectral lines. For example, for $n = 2$, a quadratic transformation (like the squared signal or the product of the signal with a delayed version of itself) will generate spectral lines Gardner (1994).

For the simplest case, which is $n = 2$, this means that a signal $x(t)$ is cyclostationary with cycle frequency α if and only if atleast some of its delay product waveforms, $y(t) = x(t-\tau)x(t)$ or $z(t) = x(t-\tau)x^*(t)$ (where $(.)^*$ denotes conjugation) for some delays τ, exhibit a spectral line at frequency α.

2.2 Cyclic Autocorrelation funtion

A zero mean process $x(t)$ is said to be cyclostationary (in the wide sense) if its autocorrelation function is a periodic function of time Gardner (1988),

$$R_x(t+\tau/2, t-\tau/2) = R_x(t+T_0+\tau/2, t+T_0-\tau/2) \tag{2.1}$$

for some period $T_0 \neq 0$ where

$$R_x(t+\tau/2, t-\tau/2) = E\{x(t+\tau/2, t)x^*(t-\tau/2, t)\} \tag{2.2}$$

and E$\{\cdot\}$ denotes mathematical expectation operation.

Since R_x is periodic, it can be represented as a fourier series as below,

$$R_x(t+\tau/2, t-\tau/2) = \sum_{\alpha} R_x^{\alpha}(\tau) e^{j2\pi\alpha t} \tag{2.3}$$

where the sum over α includes all integer multiples of the reciprocal of the fundamental period T_0. The fourier coefficients $R_x^{\alpha}(\tau)$ are given by,

$$R_x^{\alpha}(\tau) = \lim_{T\to\infty} \frac{1}{T} \int_{-\frac{T}{2}}^{\frac{T}{2}} x(t+\tau/2, t) x^*(t-\tau/2, t) e^{-j2\pi\alpha t} dt \tag{2.4}$$

2.3 Cyclic Spectrum

The Cyclic autocorrelation function is not identically zero for for all nonzero α if and only if the autocorrelation contains an additive periodic component, which will be the case if $x(t)$ is cyclostationary. The set of α values for which the Cyclic autocorrelation function is nonzero is called as the set of cyclic frequencies. The fourier transform of the cyclic autocorrelation function is called Cyclic Spectrum Gardner (1988), and is given as follows,

$$S_x^{\alpha}(f) = \int_{-\infty}^{\infty} R_x^{\alpha}(\tau) e^{-j2\pi f\tau} d\tau \tag{2.5}$$

this function can also be interpreted as a Spectral Correlation function (SCF) according to the following characterization,

$$S_x^{\alpha}(f) = \lim_{T\to\infty} \lim_{\Delta t\to\infty} \frac{1}{T\Delta t} \int_{-\frac{\Delta t}{2}}^{\frac{\Delta t}{2}} X_T(t, f+\frac{\alpha}{2}) X_T^*(t, f-\frac{\alpha}{2}) dt \tag{2.6}$$

where,

$$X_T^{(t,v)} = \int_{t-\frac{T}{2}}^{t+\frac{T}{2}} x(u) e^{-j2\pi vu} du \tag{2.7}$$

is the complex envelop of the spectral component of $x(t)$ at frequency v with ap-

proximate bandwidth $1/T$.

These two functions CAF and SCD are used to detect the hidden periodicities in modulated signals. These are observed along cyclic frequency axis for non-zero components, which indicates the cyclostationary property.

CHAPTER 3

Detection of modulated signals using Spectral Correlation Denisity function

Cyclic spectral analysis algorithms which are used to generate SCD functions generally fall into two classes, those that average in time (time smoothing) and those that average in frequency (frequency smoothing). Time smoothing algorithms are considered to be more computationally efficient for generel cyclic spectral analysis.

The time smoothed cyclic cross periodogram can be modified as Roberts *et al.* (1991),

$$S^{\alpha}_{xy_T}(n,f)_{\Delta t} = \frac{1}{T}\langle X_T(n, f+\frac{\alpha}{2}) Y^*_T(n, f-\frac{\alpha}{2})\rangle_{\Delta t} \tag{3.1}$$

where Δt represents the data time span, and $X_T(n, f+\frac{\alpha}{2})$, $Y_T(n, f-\frac{\alpha}{2})$ are the complex demodulates of narrowband and bandpass components of the signlas $x(n)$ and $y(n)$ respectively. These complex demodulates are computed in the following way Roberts *et al.* (1991),

$$X_T(n,f) = \sum_{r=-N'/2}^{r=N'/2} a(r)x(n-r)e^{-j2\pi f(n-r)T_s} \tag{3.2}$$

$$Y_T(n,f) = \sum_{r=-N'/2}^{r=N'/2} a(r)y(n-r)e^{-j2\pi f(n-r)T_s} \tag{3.3}$$

where $a(r)$ is a data tapering window of length $T = N'T_s$ seconds, with T_s being the sampling period. The fourier transform of $a(r)$ plays the role of a spectral window. A data tampering window whose fourier transform has low sidelobes (e.g., the Hamming window) is desirable.

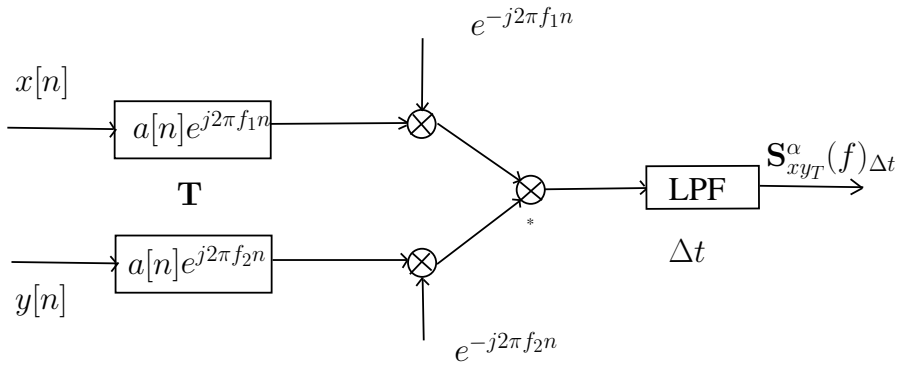

Figure 3.1: Time smoothed cyclic cross periodogram

Fig:3.1 shows a basic implementation of discrete time smoothed cyclic cross periodogram, where the symbol $*$ represents complex conjugation. The complex demodulate frequencies f_1 and f_2 are related to the spectrum frequency f and the cyclic frequency α of the point estimate by the following two equations,

$$f = \frac{f_1 + f_2}{2} \tag{3.4}$$

$$\alpha = f_1 - f_2 \tag{3.5}$$

3.1 FFT Accumulation Method

FFT Accumulation Method (FAM) algorithm is used to draw the Cyclic Spectral Plane which is described in the above section. The implementation of this algorithm is refered from Carter (1992).

Consider there are N input data samples. From the input sample data, arrays of the lengths $N^{'}$ are formed. The starting point of each succeeding row is offset from its previous row by L samples. The value of L is chosen to be $N^{'}/4$ since it allows for a good compromise between maintaining computational efficiency and minimizing cycle leakage. The value of $N^{'}$ to be determined according to the desired frequency

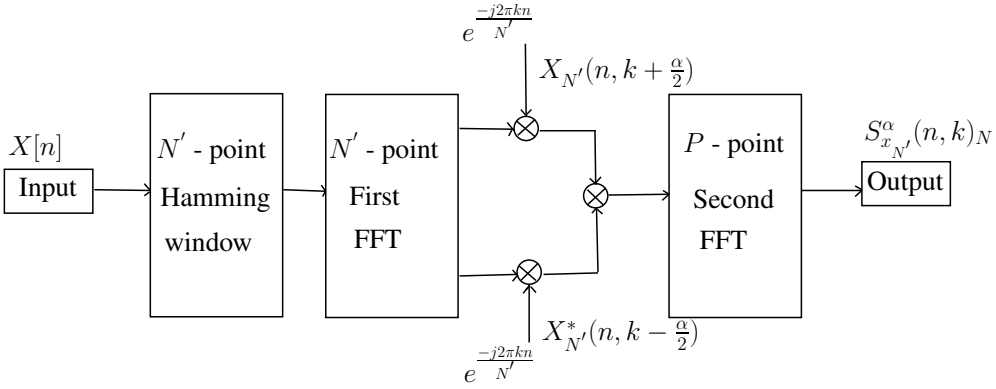

Figure 3.2: FAM algorithm block diagram

resolution (Δf), and is given by

$$N' = \frac{f_s}{\Delta f} \tag{3.6}$$

N' is chosen to be the power of 2 to take the advantage of FFT algorithm without making use of zero-padding. Thus we can form $P = \frac{N-N'}{L} \approx \frac{N}{L}$ rows. A hamming window is applied across each row, then fast fourier transformed and downconverted to baseband. Now we got an 2-D array where columns representing the constant frequencies. Each column now is point-wise multiplied with conjugate of every other column. Each resultant vector now contains P elememts and is fast fourier transformed. The lower frequency half is placed into the final Cyclic spectral plane at appropriate locations. These implementation steps are shown in the block diagram Fig:3.2.

3.2 SCD of some Modulated signals

In this section the simulated results of some modulated signals are presented.

3.2.1 AM DSBSC and SSB signals

Condider an Amplitude modulated DSBSC signal with a carrier frequency of f_c and message frequency of f_m. The spectral correlation denisity of this signal can be derived from (2.6) and can be plotted using FAM algorithm. Fig:3.3 is plotted by taking

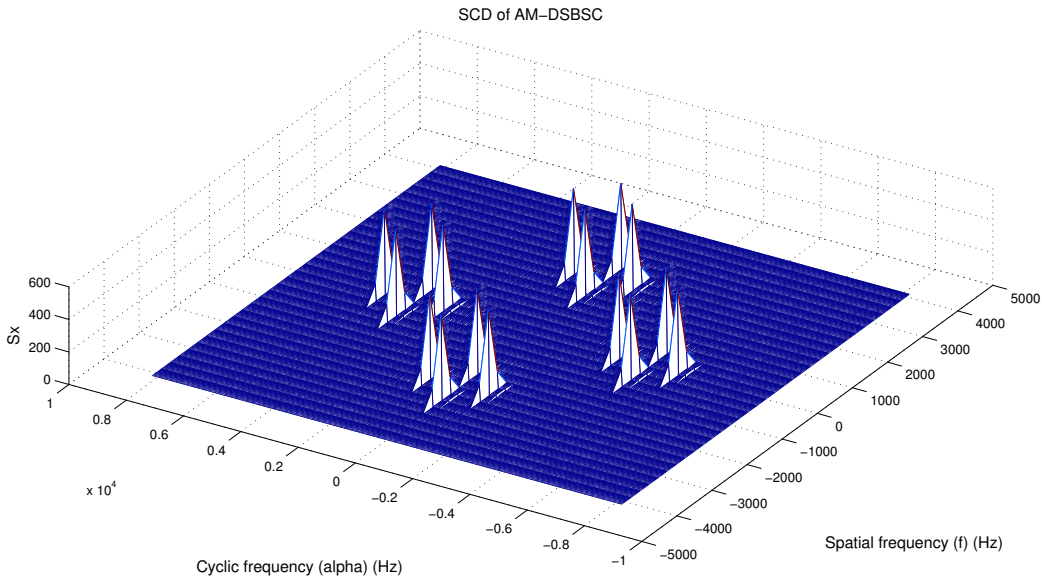

Figure 3.3: Spectral correlation denisity of AM-DSBSC signal

carrier frequency $f_c = 2048Hz$, message signal frequency $f_m = 512Hz$ and sampling frequency $f_s = 8192Hz$. Resolution in spatial frequency is $\Delta f = 256Hz$ and in cyclic frequency is $\Delta f = 32Hz$. From the Fig:3.3, we can observe that there are some non-zero components at $\alpha \neq 0$ in SCD, which are at $2f_m$,$2f_c$,$2(f_c + f_m)$ and $2(f_c - f_m)$. This components at $\alpha \neq 0$ are caused by the hidden sine-wave components. The Power spectral denisity (PSD) of the signal can be obtained by making $\alpha = 0$.

Similarly Fig:3.4 is plotted for AM-SSB signal.

3.2.2 OFDM signals

OFDM signals exhibit cyclostationarity due to severel reasons. It may be by the pilot subcarriers or by the cyclic prefix. We can make OFDM signal as cyclostationary by unique embedded signatures also.

The SCD of an OFDM signal is simulated, which exhibits cyclostationarity due to periodically induced pilot subcarriers Schnur (2009). A signal of length 256 OFDM symbols is taken, in which each OFDM symbol contains 64 subcarriers along with a CP of 16 subcarriers. 12 subcarriers are reserved for guardband and no symbols are transmitted through them. 4 subcarriers are used for pilot symbools which are BPSK

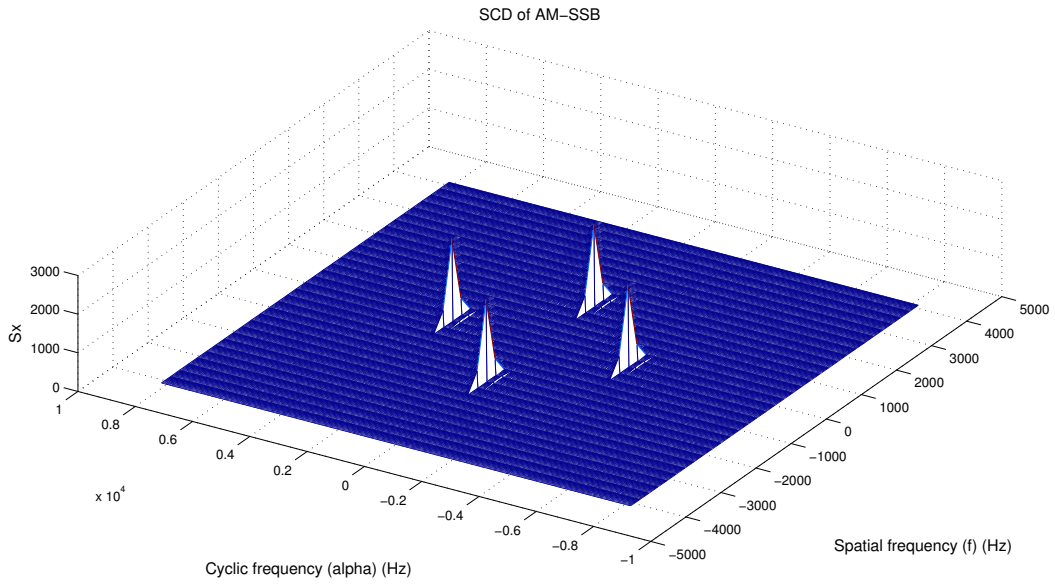

Figure 3.4: Spectral correlation denisity of AM-SSB signal

modulated and remaining 48 subcarriers are used for data symbols which are taken from 16-QAM. 4 subcarriers are placed at a positions of -21,-7,7,21 in a symbol which are equally spaced. These pilot subcarriers cause the cyclostationary signature which can be observed from SCD function. The SCD of this signal at $f = 0$ is presented in Fig:3.5, where we can observe the peaks at regular intervals along the α axis due to pilot subcarriers.

The position of the peaks depends on the location of the pilot subcarriers in the OFDM symbol. This is shown in Fig:3.6. In figure 1, pilots are placed at positions of -21,-7,7,21 in OFDM symbol. The peak corresponds to third pilot can be seen at $\frac{7}{32} \times 2 \times 10^7 Hz$ which is 4.375 MHz. Whereas in figure 2, pilots are placed at positions of -9,-3,3,9 in OFDM symbol. The peak corresponds to third pilot can be seen at $\frac{3}{32} \times 2 \times 10^7 Hz$ which is 1.875 MHz. This distinguish feature caused by pilots, which can be captured through SCD function can be useful in the interception of OFDM signals.

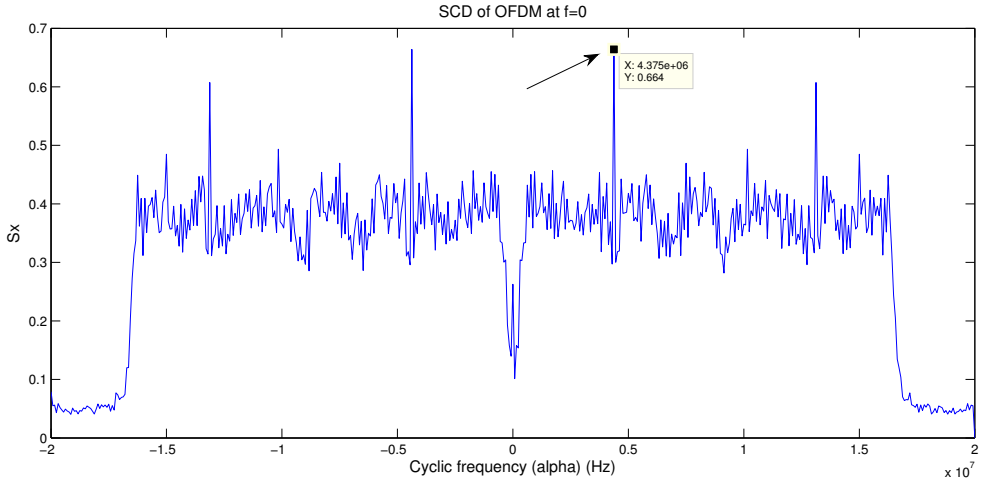

Figure 3.5: Spectral correlation denisity of OFDM signal at $f = 0$

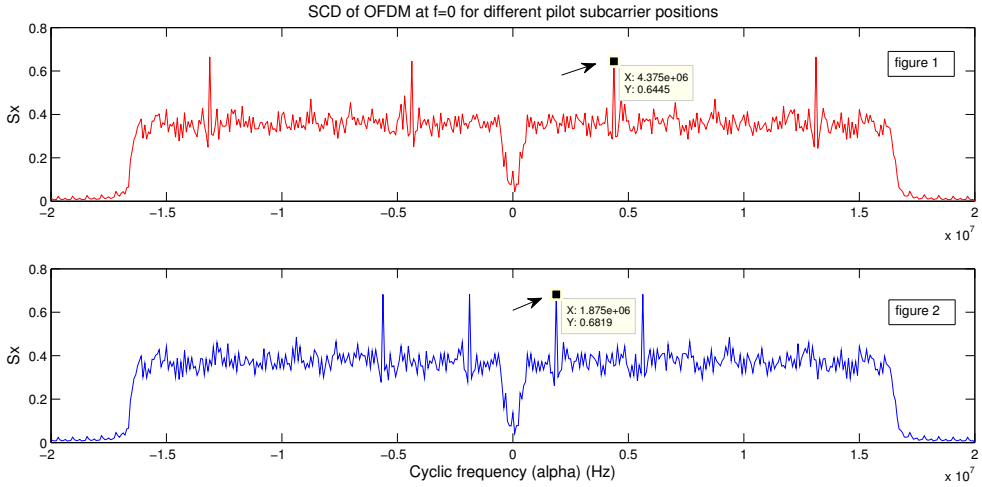

Figure 3.6: Spectral correlation denisity of OFDM signal at $f = 0$ for different pilot subcarrier positions

CHAPTER 4

Introduction to LTE OFDM signal Model

LTE is a standard in wireless communications for high-speed data transfer rates. The standard is developed by the 3GPP (3rd Generation Partnership Project). The LTE specification provides downlink peak rates of 300 Mbit/s, uplink peak rates of 75 Mbit/s. LTE has the ability to manage fast-moving mobiles and supports multi-cast and broadcast streams. LTE supports scalable carrier bandwidths, from 1.4 MHz to 20 MHz and supports both frequency-division duplexing (FDD) and time-divisionduplexing (TDD). It uses Orthogonal frequency Division Multiple Access (OFDMA) on the downlink (DL) and Single Carrier- Frequency Division Multiple Access (SC-FDMA) on the uplink (UL). In this thesis, we consider the detection of Downlink signals using the Cyclostationary property of OFDM signals.

4.1 LTE Frame structure

The time domain structure for LTE transmission contains frames of length 10 ms consisting of ten equally sized subframes of length 1 ms Dahlman *et al.* (2010). In case of FDD operation, there are two carrier frequencies, one for uplink transmission (f_{UL}), and one for downlink transmission (f_{DL}). In case of TDD operation, there is only a single carrier frequency, and uplink and downlink transmissions are separated in time. Each subframe contains two slots, and each of duration 0.5 ms. Each slot contains N_{symb}^{DL} OFDM symbols. The number of OFDM symbols in a slot depends on the length of cyclic prefix. The non-MBSFN mode employs subcarrier spacing of 15 kHz and either short or long CP, where for the short CP $N_{symb}^{DL} = 7$ and for the long CP $N_{symb}^{DL} = 6$.

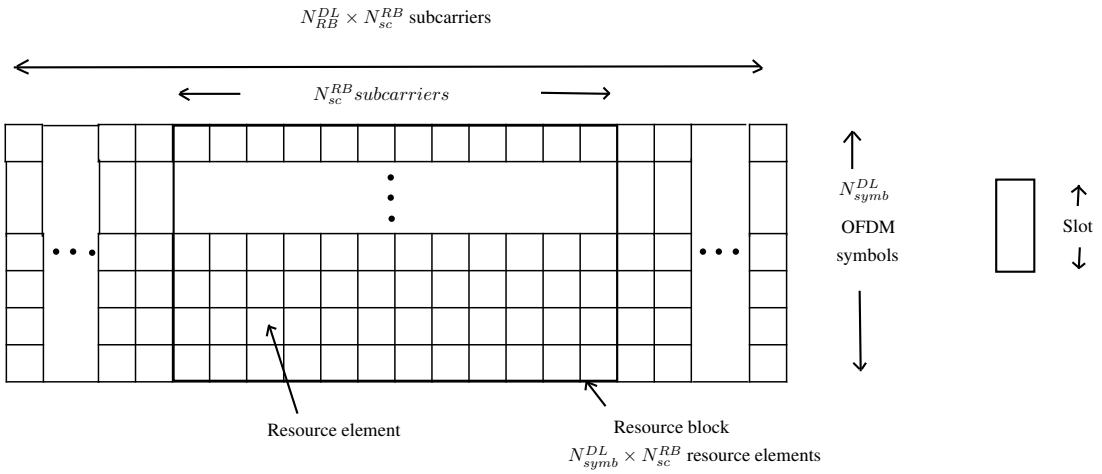

Figure 4.1: Slot structure and physical resource block in the FDD downlink frame

4.2 Slot structure and physical resource elements

The transmitted signal in each slot is described by a resource grid of N_{symb}^{DL} OFDM symbols and N_{RB}^{DL} N_{sc}^{RB} subcarriers for each symbol. The no. of subcarriers per resource block (N_{sc}^{RB}) is 12 and 24 for the LTE signals with the subcarrier spacing of 15 kHz and 7.5 kHz respectively. The total number of resource blocks N_{RB}^{DL} varies with the downlink transmission bandwidth and it ranges from 6 to 110, which are the smallest and largest bandwidths respectively. So the transmission bandwidth varies from 1.4 MHz to 20 MHz.

Each element in a resource grid is called a resoure element and is identified by the index pair (k, l) in a slot, where $k = 0$ to N_{RB}^{DL} N_{sc}^{RB} -1 and $l = 0$ to $N_{symb}^{DL} - 1$ are the indices in frequency and time domain respectively. A physical resource block consists of $N_{symb}^{DL} \times N_{sc}^{RB}$ resource elements, corresponding to one slot in time domain and 180 kHz in frequency domain. Fig:4.1 shows the slot structure Zyren and McCoy (2007).

4.3 Reference Signals

Reference signals are embedded in the resource blocks of the transmission frame for channel estimation and cell search. There are three types of downlink reference signal for LTE.

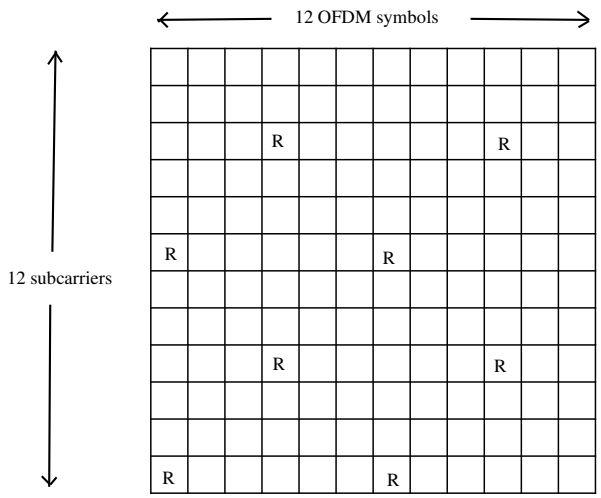

Figure 4.2: Reference signals in physical resource blocks

1. Cell specific reference signals, associated with non-MBSFN transmission.
2. MBSFN reference signals, associated with MBSFN transmission.
3. UE-specific reference signals.

A brief discussion on Cell specific reference signals is presented as they were used in simulations. The RSs are usually transmitted on some of the subcarriers of one or two non-consecutive symbols in each slot. An example is provided in the Fig:4.2 for long CP ($N_{symb}^{DL} = 6$ OFDM symbols) over one resource block and two consecutive slots Zyren and McCoy (2007). from the figure, we can observe that the RS is transmitted over first and seventh subcarriers of the first OFDM symbol and on the fourth and tenth subcarriers of the fourth OFDM symbol in each slot.

CHAPTER 5

Detection of LTE Signals using CAF

In this chapter detection of LTE OFDM signals is simulated using CAF. A generel model for LTE signal with any RS distribution is provided. The continuous-time signal affected by additive Gaussian noise can be expressed as Al-Habashna *et al.* (2010),

$$
\begin{aligned}
r(t) = a[& \sum_{\substack{l=-\infty \\ l \bmod N_z \in Z_1}}^{\infty} \sum_{\substack{k=-K/2, k\neq 0 \\ k \notin A_1}}^{K/2} b_{k,l} g(t-lT) e^{j2\pi k\Delta f\ (t-lT)} \\
& + \sum_{\substack{l=-\infty \\ l \bmod N_z \in Z_1}}^{\infty} \sum_{\substack{k=-K/2, k\neq 0 \\ k \in A_1}}^{K/2} c_{k,l} g(t-lT) e^{j2\pi k\Delta f\ (t-lT)}] \\
& + a[\sum_{\substack{l=-\infty \\ l \bmod N_z \in Z_2}}^{\infty} \sum_{\substack{k=-K/2, k\neq 0 \\ k \notin A_2}}^{K/2} b_{k,l} g(t-lT) e^{j2\pi k\Delta f\ (t-lT)} \\
& + \sum_{\substack{l=-\infty \\ l \bmod N_z \in Z_2}}^{\infty} \sum_{\substack{k=-K/2, k\neq 0 \\ k \in A_2}}^{K/2} c_{k,l} g(t-lT) e^{j2\pi k\Delta f\ (t-lT)}] \\
& + a \sum_{\substack{l=-\infty \\ l \bmod N_z \notin Z_1, Z_2}}^{\infty} \sum_{k=-K/2, k\neq 0}^{K/2} b_{k,l} g(t-lT) e^{j2\pi k\Delta f\ (t-lT)} + w(t) \quad (5.1)
\end{aligned}
$$

where a is the amplitude factor, N_z is the repetition period for RS distribution, Z_1 and Z_2 are the stes of OFDM symbols in which the RSs is transmitted, A_1 and A_2 are the sets of subcarriers on which the RSs is transmitted in the OFDM symbols belonging to Z_1 and Z_2 respectively, T is the OFDM symbol period, $g(t)$ is the impulse response, $b_{k,l}$ and $c_{k,l}$ are the data and RS symbols transmitted on the kth subcarrier and within lth OFDM symbol respectively and $w(t)$ is the additive zero-mean gaussian noise.

5.1 Theoritical plots of CAF magnitude Vs CF

The discrete time LTE OFDM signal, $r(n)$, exhibits RS-induced second order cyclo-stationarity. According to the derivations from Al-Habashna *et al.* (2010), the Cyclic Autocorrelation Function (CAF) at Cyclic frequency (CF) α and delays equal to integer multiples of the frame duration, D_F is given by

$$R_r^{\alpha}(\tau) = D_z^{-1} a^2 \sigma_c^2 K_r [\sum_{s \epsilon Z_1} e^{-j2\pi\alpha sD} + \sum_{s \epsilon Z_2} e^{-j2\pi\alpha sD}] \times \sum_{n} |g(n)|^2 e^{-j2\pi\alpha n} \tag{5.2}$$

where

$$\alpha : \alpha = vD_z^{-1}, vinteger \tag{5.3}$$

$D_z = T_z f_s$ – no. of samples over T_z

T_z – time period correspond to N_z OFDM symbols

$D = T f_s$ – no. of samples over T

σ_c^2 – Variance of the RS symbols

K_r – The no. of reference signal subcarriers

based on equations (5.2) and (5.3), The plots of CAF magnitude Vs CF are presented in Fig:5.1 and Fig:5.2

5.2 Simulated results of Probability of detection Vs SNR

From the results in above section, for LTE signals, we can observe some non-zero values of CAF at CF $\alpha = 0$ and delay $\tau = D_F$. If we detect that α is a CF for the delay D_F, we can decide that an LTE OFDM signal is present. to detect second-order CF, a statstical

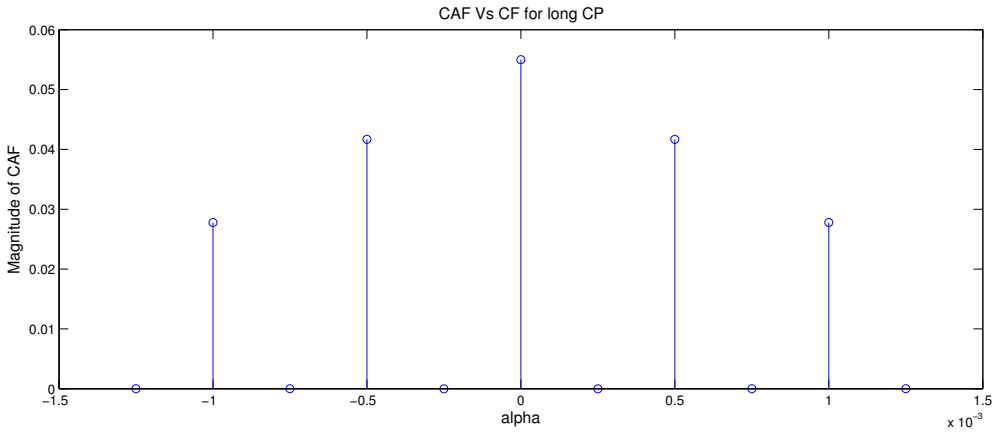

Figure 5.1: The CAF magnitude Vs CF at delay equal to D_F for the LTE OFDM signals with non-MBSFN mode (cell-specific RS) and long CP

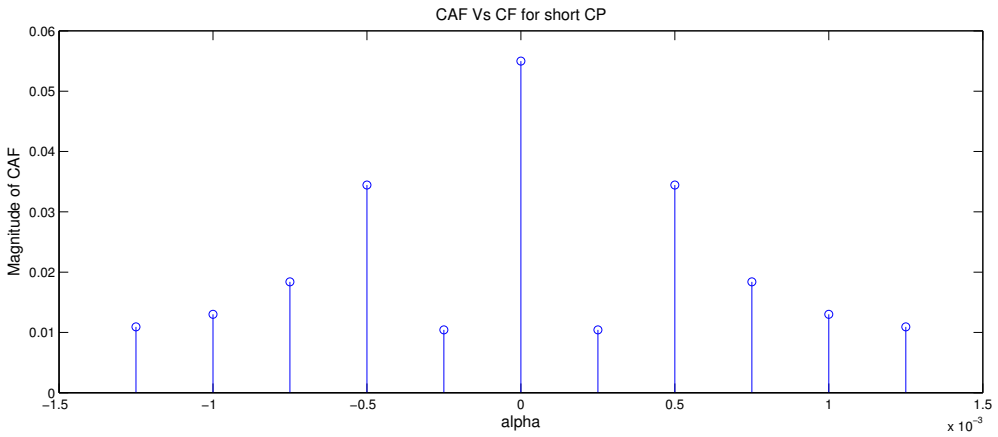

Figure 5.2: The CAF magnitude Vs CF at delay equal to D_F for the LTE OFDM signals with non-MBSFN mode (cell-specific RS) and short CP

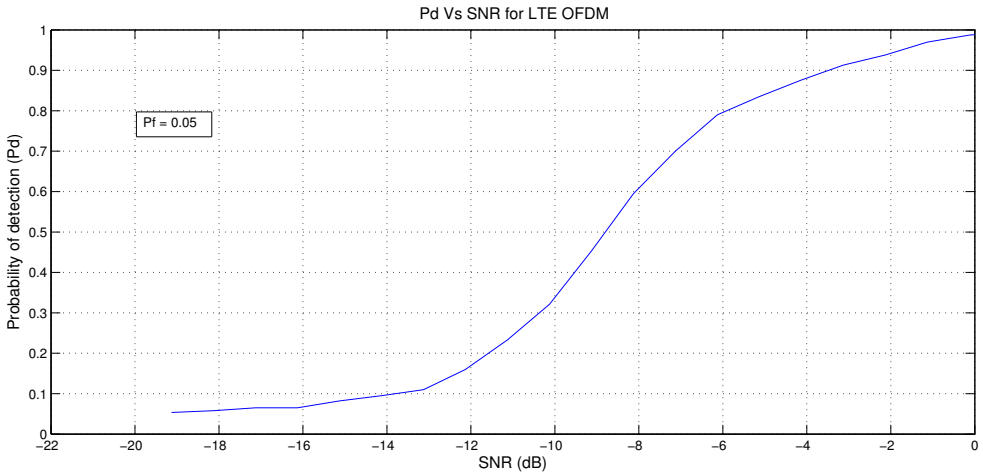

Figure 5.3: Probability of detection Vs SNR for the LTE OFDM signals

test is developed in Dandawate and Giannakis (1994).

According to Dandawate and Giannakis (1994), this detection problem can be modeled as a binary hypothesis testing problem. We decide the CF based on the magnitude of CAF. Under hypothesis H_0 α is not a CF and under H_1 α is a CF. The CAF of the received signal $r(n)$ is estimated at frequency α and at delay τ, and a vector $\hat{\mathbf{R}}_{\mathbf{r}}^{\alpha}$ is formed.

$$\hat{\mathbf{R}}_{\mathbf{r}}^{\alpha} = [\mathbf{Re}\{\hat{\mathbf{R}}_{\mathbf{r}}^{\alpha}(\tau)\}\mathbf{Im}\{\hat{\mathbf{R}}_{\mathbf{r}}^{\alpha}(\tau)\}], \tag{5.4}$$

where $Re\{\cdot\}$ and $Im\{\cdot\}$ are the real and imaginary parts respectively. The test statistic can be computed as follows,

$$\mathbf{\Psi}_{\mathbf{r}}^{\alpha} = \mathbf{N_s}\hat{\mathbf{R}}_{\mathbf{r}}^{\alpha}\hat{\mathbf{\Sigma}}^{-1}\hat{\mathbf{R}}_{\mathbf{r}}^{\alpha\dagger} \tag{5.5}$$

where -1 and † denotes the matrix inverse and transpose respectively and $\hat{\Sigma}$ is an estimate of the covariance matrix of $\hat{\mathbf{R}}_{\mathbf{r}}^{\alpha}$ Dandawate and Giannakis (1994). This test statistic is compared against a threshold Γ and if $\mathbf{\Psi}_{\mathbf{r}}^{\alpha} \geq \mathbf{\Gamma}$, we can decide that α as CF, otherwise it is not.

The simulated result for Probability of detection Vs SNR is presented in the Fig:5.3 for LTE OFDM signals. No. of resource blocks considered are 6 which is minimum in

LTE standard. LTE OFDM signal is observed for 2 frames, which is of 20 msec. Long CP is used, so the no. of OFDM symbols per slot is 6. Data symbols are taken from QPSK, and reference symbols are BPSK modulated. Reference symbols are distributed as shown in Fig:4.2. The probability of detection is plotted for SNRs ranging from 0 dB to -20 dB for the Probability of false alarm of 0.05.

CHAPTER 6

OFDM signal detection

In the previous chapter detection of LTE OFDM signal has been shown. In this chapter we will see the cyclostationarity induced by CP of OFDM signals and some improvements in the detection performance through decimation Turunen *et al.* (2009) and sensing time Al-Habashna *et al.* (2010) are simulated. A blind detection of FFT length of OFDM symbol is also provided. The detection performance is also verified for multipath channels.

The discrete time equivalent of (2.4), to obtain the cyclic spectrum of a modulated signal is given by,

$$\mathbf{R}_x^{\alpha} = \frac{1}{N}\sum_{n=0}^{N-1} x(n)x^*(n-\tau)e^{-j2\pi\alpha n/N} \tag{6.1}$$

The cyclic spectrum of OFDM signal can be computed with the help of (6.1). Peaks are observed along the α-axis, due to the CP of OFDM signal. So the detection performance varies with the length of CP. As length of the CP reduces, detection performance will get worse. It can be seen in the Fig:6.1. The cyclic spectrum is simulated for OFDM signal with 100 symbols, where each symbol contains 64 subcarriers at SNR of 0 dB. In figure 1, length of CP is taken as 16 subcarriers and in figure 2, length of CP is 8 subcarriers. We can see that the peaks are more significant for the long CP.

6.1 OFDM signal detection performance with the decimation ratio

Often the case is that the information in the cyclic spectrum resides on lower frequencies. So the information at higher frequencies is of no interest, and the autocorrelation product can be resampled at lower frequencies, by eliminating higher frequencies. This

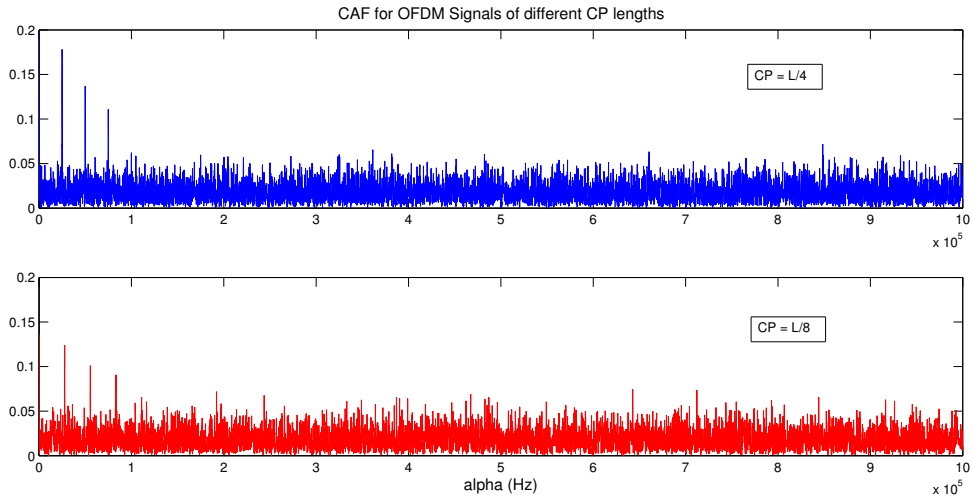

Figure 6.1: Cycle spectrum of OFDM signal for different CP lengths

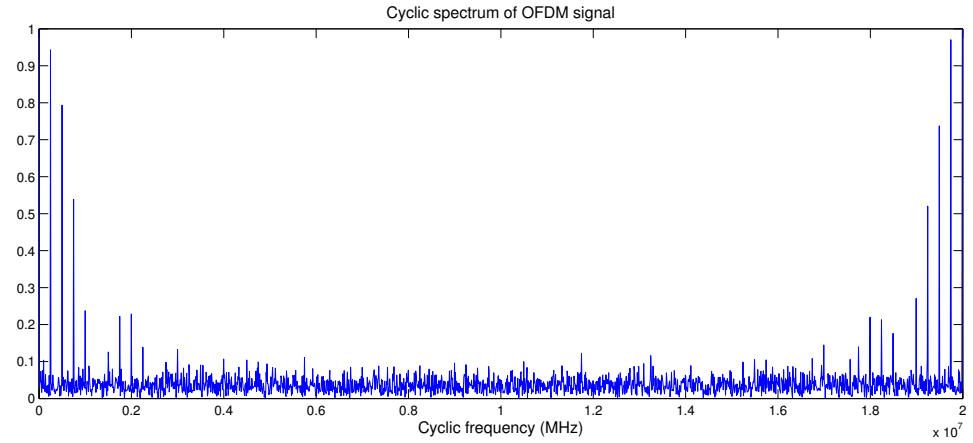

Figure 6.2: Cycle spectrum of OFDM sampled at 20 MHz

is illustrated in Fig:6.2 and Fig:6.3. an OFDM signalsampled at 20 MHz is taken, which contains 64 subcarriers and a CP of 16 subcarriers for each symbol. The cyclic spectrum of this signal is shown in Fig:6.2. The simulation is repeated by applying a decimation factor of 8, and the modified cyclic spectrum is shown in Fig:6.3.

Detection time, that is the time interval over which the test statistic is calculated from input samples is given by Turunen *et al.* (2009),

$$T_d = \frac{M * N_{FFT}}{f_{s,in}} \tag{6.2}$$

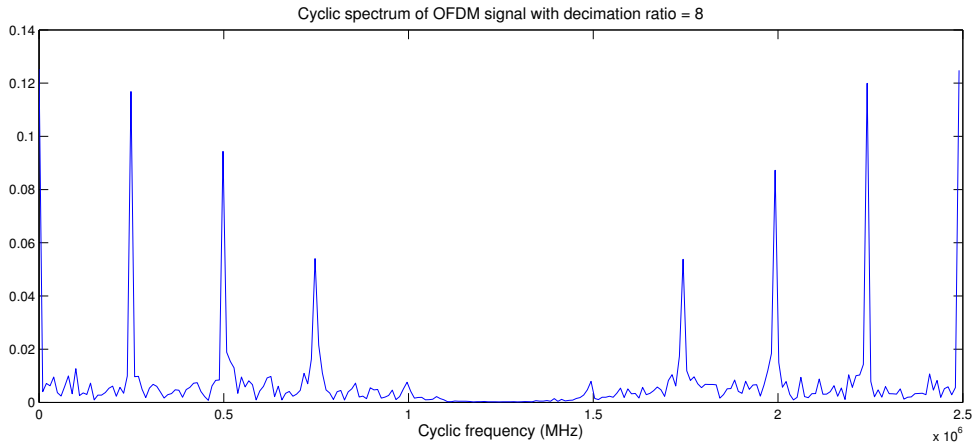

Figure 6.3: Modified cyclic spectrum with decimation ratio of 8

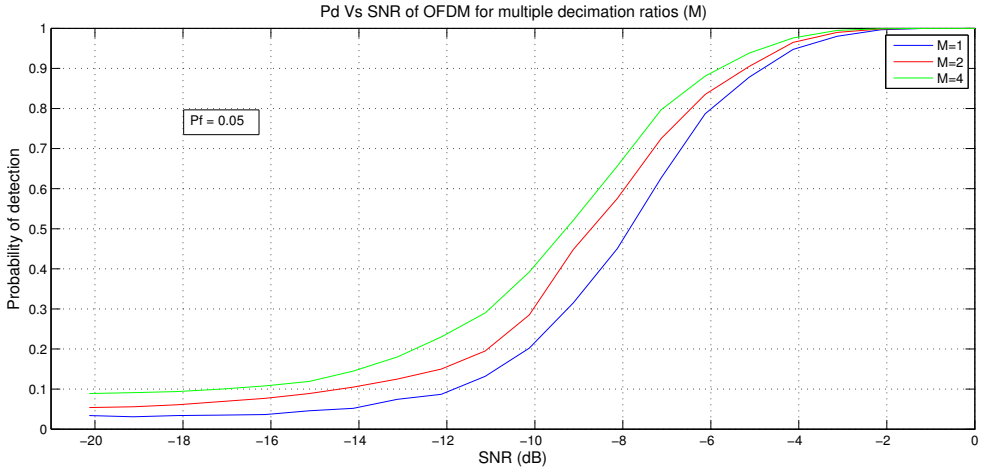

Figure 6.4: Probability of detection Vs SNR for the OFDM signals for multiple decimation ratios

where $f_{s,in}$ is the input sampling frequency, M is the decimation ratio and N_{FFT} is 2048. So by keeping N_{FFT} as constant, detection time can be increased with the decimation ratio M, which in turn increases the detection performance.

The simulated result is presented in Fig:6.4. An OFDM signal is taken with 200 OFDM symbols, where there are 64 subcarriers and a CP of 16 subcarriers for each OFDM symbol. Subcarrier modulation employed is 16-QAM. Probability of detection is plotted for the Probability of false alarm of 0.05. From the Fig:6.4 we can conclude that detector performance is increasing with increase in decimation ratio.

Maximum decimation ratio depends on cyclic frequencies of signal under detection or could also be limited by detection time constraints.

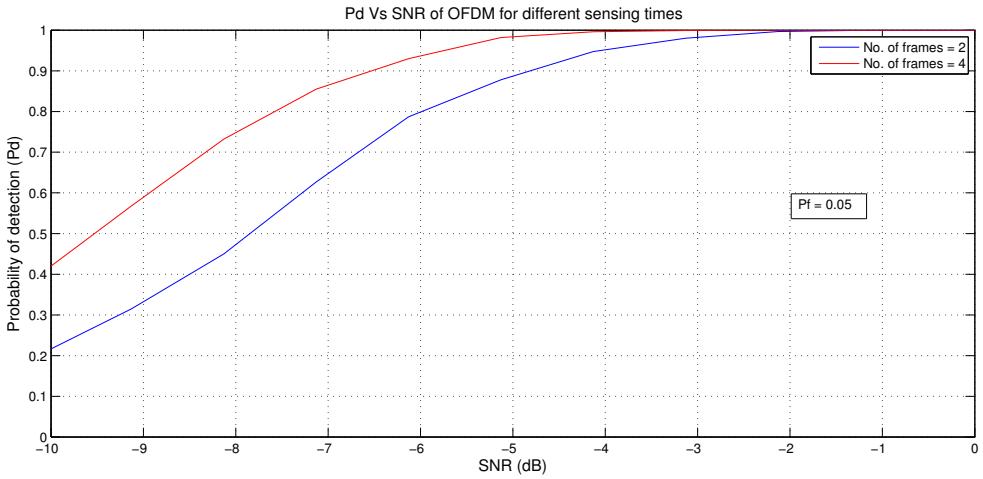

Figure 6.5: Probability of detection Vs SNR for the OFDM signals for different sensing times

6.2 OFDM signal detection performance with sensing time

Fig:6.5 shows the detector performance for different sensing times. The detector performance improves with an increase in the sensing time as expected Al-Habashna *et al.* (2010). Probability of detection is plotted against SNR for two different frame lengths of 2 and 4. Each frame contains 100 OFDM symbols and each symbol carries a total of 80 subcarriers along with the CP.

6.3 Blind detection of FFT length of OFDM signal

The cyclic spectrum of OFDM signal can also be used to detect the FFT length used in OFDM. The position of first peak occurs at a cycle frequency of $\frac{f_s}{N_{FFT}+L_{CP}}$, where f_s is the sampling frequency, N_{FFT} is the FFT length taken for OFDM modulation and L_{CP} is the length of CP. An OFDM signal is taken with N subcarriers and cyclic prefix of length $N/4$ and is sampled at 20 MHz. The simulated result is presented for $N = 128$, and 128-point IFFT is applied at the transmiter end. We can observe the first peak at $\frac{fs}{160}$, which is 12500 Hz in Fig:6.6.

This may be used in the detection between Wi-Fi and LTE signals as the FFT-lengths

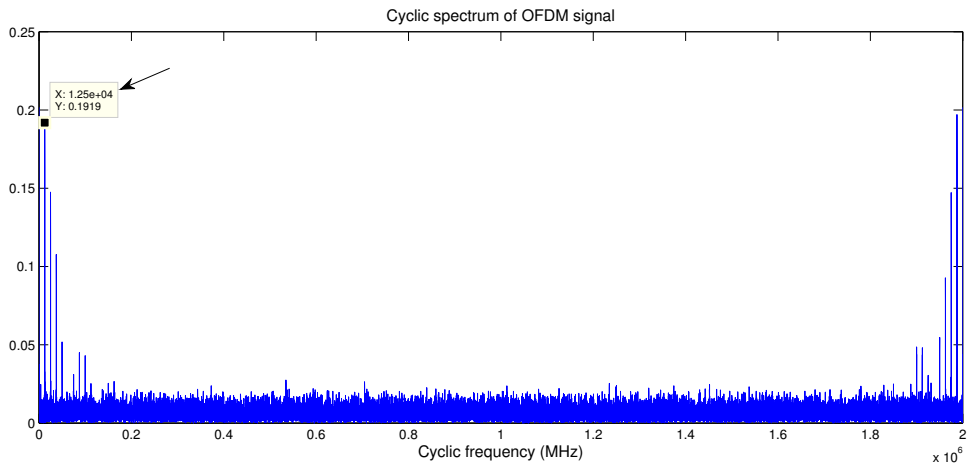

Figure 6.6: Detection of FFT length through cyclic spectrum of OFDM

of their OFDM signals are different. Wi-Fi uses 64-FFT, whereas LTE signal ranges it from 128 to 2048.

6.4 OFDM signal detection performance in multi-path channel

Till now we discussed the detection performance of this method in single-tap channel. In this section we see the detector performance for multi-tap channel. The expression for CAF of a signal $x(n)$ is given by (6.1). Assume a signal $x(n)$ is passed through a channel with L-taps and the channel response is given by $h(n)$, and let $y(n) = x(n) * h(n)$, then the expression for CAF can be modified, and is given by

$$\mathbf{R}_y^\alpha = (\sum_{l=0}^{L-1} |h(l)|^2) \times \mathbf{R}_x^\alpha \tag{6.3}$$

The derivation for this expression is carried out in Appendix A.

The simulations for OFDM signal detection are performed for channel with 3-taps and unit energy which is given by,

$$h(n) = 0.8729\delta(n) + 0.4364\delta(n-1) + 0.2182\delta(n-2)$$

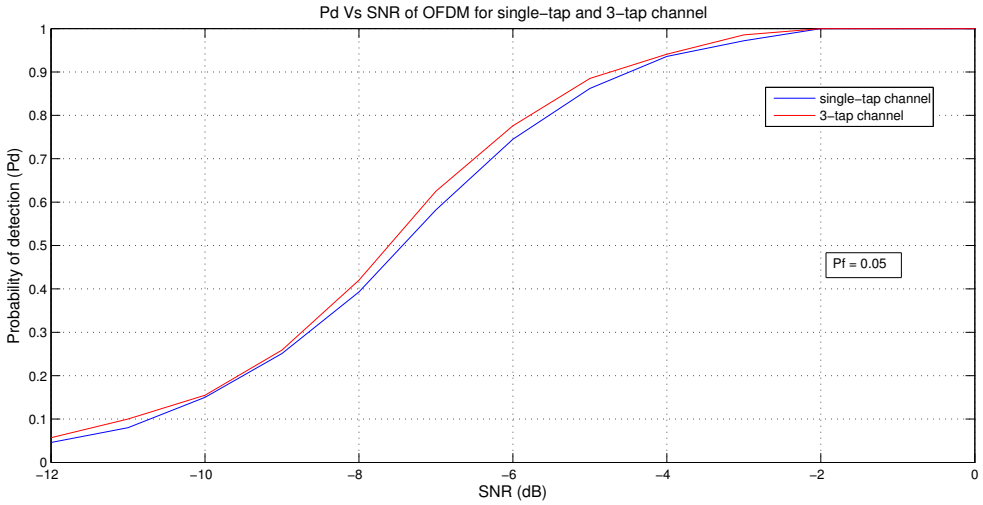

Figure 6.7: Probability of detection Vs SNR for the OFDM signals for single and 3-tap channels

The OFDM signal contains 200 OFDM symbols, whereas each symbol contains 64 subcarriers and a CP of 16 subcarriers. Each data subcarrier is 16-QAM modulated. From the Fig:6.7, it can be deduced that the detection performance is almost same as the channel with single tap, which is valid according to (6.3). The simulation is to be done for more number of iterations for convergence of those two curves.

From (6.3), we can say that channel with multiple-taps don't alter the cyclic spectrum except for scaling Because the CAF function is just scaled by the energy of the channel, which results in increasing or decreasing the peaks in CAF, the detection performance can be affected. So the detection performance varies directly with the channel energy. The CAF is simulated for another channel (Fig:6.8) which is given by,

$$h(n) = 0.65\delta(n) + 0.325\delta(n-1) + 0.1625\delta(n-2)$$

From the Fig:6.8, we can observe that amplitudes are scaled by energy of the channel. In single-tap channel the amplitude of first peak is 0.1917, and for 3-tap channel it is 0.1178, which is 0.1917×0.5545, where 0.5545 is the energy of the channel.

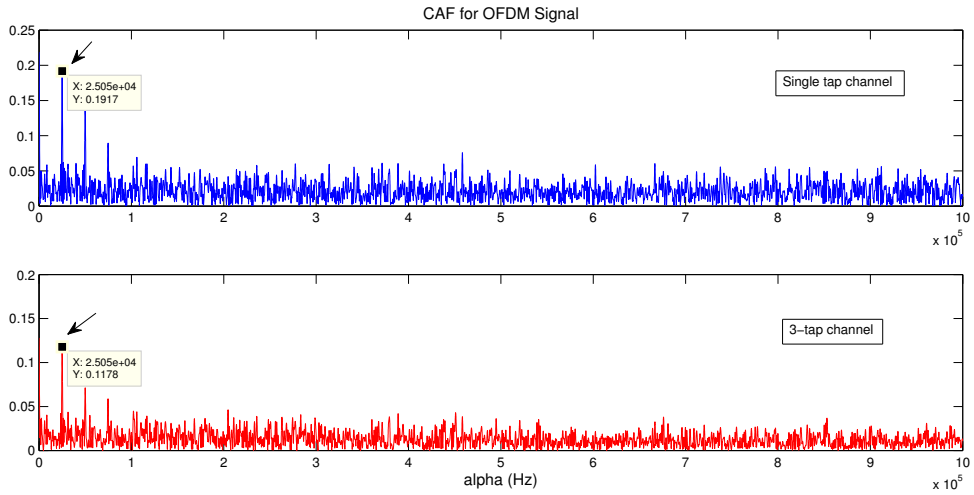

Figure 6.8: Cyclic spectrum of OFDM for different channel responses

CHAPTER 7

Conclusion and Future work

This thesis discussed the fundamentals of Cyclostationary property and LTE OFDM signals. The cyclostationary property of different modulated signals is observed by the simulations of SCD using FAM algorithm. For OFDM signals it is shown how pilot subcarriers induces cyclostationarity and how it changes with the position of pilots through SCD function. The Cyclic Autocorrelation function of OFDM signals is simulated and has been used in the detection of those signlas. The CAF function captures cyclostationary signature caused by the CP of OFDM signals. It has been shown that detection performance varies with the length of CP, decimation ratio and with the sensing time. The simulated CAF is used in the blind detection of FFT length of OFDM which may be used in the detection between Wi-Fi and LTE. The cyclic spectrum for multi-path channel is derived and the effect of channel taps on the detection performance is explained. The simulation results are shown and found matching with the theoritical work.

The detector performance is simulated for additive gaussian noise. This is to be done for non-white guassian noise. This method can be verified under different fading environments and for different channels.

APPENDIX A

Cyclic spectrum for a signal in multi-path channel

From (6.1) the expression for Cyclic spectrum of a signal $x(n)$ is given by,

$\mathbf{R}_x^\alpha = \frac{1}{N}\sum_{n=0}^{N-1} x(n)x^*(n-\tau)e^{-j2\pi\alpha n/N}$

Let $x(n)$ is passed through a channel with L-taps, and let $y(n) = x(n) * h(n)$, then the Cyclic spectrum for $y(n)$ can be written as,

$$\begin{aligned}\mathbf{R}_y^\alpha &= \frac{1}{N}\sum_{n=0}^{N-1} y(n)y^*(n-\tau)e^{-j2\pi\alpha n/N} \\ &= \frac{1}{N}\sum_{n=0}^{N-1}(x(n)*h(n))(x^*(n-\tau)*h^*(n-\tau))e^{-j2\pi\alpha n/N} \\ &= \frac{1}{N}\sum_{n=0}^{N-1}(\sum_{l=0}^{L-1} h(l)x(n-l))(\sum_{p=0}^{L-1} h^*(p)x^*(n-\tau-p))e^{-j2\pi\alpha n/N} \\ &= \frac{1}{N}(\sum_{l=0}^{L-1} h(l)(\sum_{p=0}^{L-1} h^*(p)(\sum_{n=0}^{N-1} x(n-l)x^*(n-\tau-p)e^{-j2\pi\alpha n/N})))\end{aligned} \tag{A.1}$$

Let $n - l = z$, then

$$\mathbf{R}_y^\alpha = \frac{1}{N}(\sum_{l=0}^{L-1} h(l)\sum_{p=0}^{L-1} h^*(p)(\sum_{z=-l}^{N-1-l} x(z)x^*(n-\tau+l-p)e^{-j2\pi\alpha(l+z)/N}))) \tag{A.2}$$

The inner summation is the Cyclic spectrum of $x(n)$, and is non zero only for the delay of τ. So by taking $l = p$, we can write,

$$\mathbf{R}_y^\alpha = (\sum_{l=0}^{L-1} |h(l)|^2) \times \mathbf{R}_x^\alpha \tag{A.3}$$

REFERENCES

1. **Al-Habashna, A.**, **O. Dobre**, **R. Venkatesan**, and **D. Popescu**, Cyclostationarity-based detection of lte ofdm signals for cognitive radio systems. *In Global Telecommunications Conference (GLOBECOM 2010), 2010 IEEE*. IEEE, 2010.

2. **Carter, N. J.** (1992). Implementation of cyclic spectral analysis methods. Technical report, DTIC Document.

3. **Dahlman, E.**, **S. Parkvall**, **J. Skold**, and **P. Beming**, *3G evolution: HSPA and LTE for mobile broadband*. Academic Press, 2010.

4. **Dandawate, A. V.** and **G. B. Giannakis** (1994). Statistical tests for presence of cyclostationarity. *Signal Processing, IEEE Transactions on*, **42**(9), 2355–2369.

5. **Gardner, W. A.** (1988). Signal interception: a unifying theoretical framework for feature detection. *Communications, IEEE Transactions on*, **36**(8), 897–906.

6. **Gardner, W. A.** (1994). Cyclostationarity in communications and signal processing. Technical report, DTIC Document.

7. **Roberts, R. S.**, **W. A. Brown**, and **H. H. Loomis Jr** (1991). Computationally efficient algorithms for cyclic spectral analysis. *Signal Processing Magazine, IEEE*, **8**(2), 38–49.

8. **Schnur, S. R.** (2009). *Identification and classification of OFDM based signals using preamble correlation and cyclostationary feature extraction*. Ph.D. thesis, Monterey, California Naval Postgraduate School.

9. **Turunen, V.**, **M. Kosunen**, **A. Huttunen**, **S. Kallioinen**, **P. Ikonen**, **A. Parssinen**, and **J. Ryynanen**, Implementation of cyclostationary feature detector for cognitive radios. *In Cognitive Radio Oriented Wireless Networks and Communications, 2009. CROWNCOM'09. 4th International Conference on*. IEEE, 2009.

10. **Zyren, J.** and **W. McCoy** (2007). Overview of the 3gpp long term evolution physical layer. *Freescale Semiconductor, Inc., white paper*.